



**HAL**  
open science

## Multi-object segmentation framework using deformable models for medical imaging analysis

Rafael Namías, Juan Pablo D'amato, Mariana del Fresno, Marcelo Vénere,  
Nicola Pirró, Marc-Emmanuel Bellemare

► **To cite this version:**

Rafael Namías, Juan Pablo D'amato, Mariana del Fresno, Marcelo Vénere, Nicola Pirró, et al.. Multi-object segmentation framework using deformable models for medical imaging analysis. *Medical and Biological Engineering and Computing*, 2016, 54 (8), pp.1181-1192. 10.1007/s11517-015-1387-3 . hal-03812641

**HAL Id: hal-03812641**

**<https://cnrs.hal.science/hal-03812641>**

Submitted on 1 Feb 2024

**HAL** is a multi-disciplinary open access archive for the deposit and dissemination of scientific research documents, whether they are published or not. The documents may come from teaching and research institutions in France or abroad, or from public or private research centers.

L'archive ouverte pluridisciplinaire **HAL**, est destinée au dépôt et à la diffusion de documents scientifiques de niveau recherche, publiés ou non, émanant des établissements d'enseignement et de recherche français ou étrangers, des laboratoires publics ou privés.

# Multi-object segmentation framework using deformable models for medical imaging analysis

Rafael Namías · Juan Pablo D'Amato · Mariana del Fresno · Marcelo Vénere · Nicola Pirró · Marc-Emmanuel Bellemare

the date of receipt and acceptance should be inserted later

**Abstract** Segmenting structures of interest in medical images is an important step in different tasks such as visualization, quantitative analysis, simulation and image-guided surgery, among several other clinical applications. Numerous segmentation methods have been developed in the past three decades for extraction of anatomical or functional structures on medical imaging. Deformable models, which include the active contour models or snakes, are among the most popular methods for image segmentation combining several desirable features such as inherent connectivity and smoothness. Even though different approaches have been proposed and significant work has been dedicated to the improvement of such algorithms, there are still challenging research directions as the simultaneous extraction of

multiple objects and the integration of individual techniques.

This paper presents a novel open-source framework called Deformable Models Array (DMA) for the segmentation of multiple and complex structures of interest in different imaging modalities. While most active contour algorithms can extract one region at a time, DMA allows integrating several deformable models to deal with multiple segmentation scenarios. Moreover, it is possible to consider any existing explicit deformable model formulation and even to incorporate new active contour methods, allowing to select a suitable combination in different conditions. The framework also introduces a control module that coordinates the cooperative evolution of the snakes, and is able to solve interaction issues towards the segmentation goal. Thus, DMA can implement complex-object and multi-object segmentation in both 2D and 3D using the contextual information derived from the model interaction. These are important features for several medical image analysis tasks in which different but related objects need to be simultaneously extracted. Experimental results on both Computed Tomography (CT) and Magnetic Resonance Imaging (MRI) show that the proposed framework has a wide range of applications especially in the presence of adjacent structures of interest or under intra-structure inhomogeneities giving excellent quantitative results.

---

R. Namías  
CIFASIS, UNR-CONICET/UAM (France), Bv 27 de febrero  
210 bis, Rosario, Argentina  
E-mail: namias@cifasis-conicet.gov.ar

J. P. D'Amato  
Consejo Nacional de Investigaciones Científicas y Técnicas  
& Instituto PLADEMA, Universidad Nacional del Centro,  
Tandil, Argentina.

M. del Fresno  
Comisión de Investigaciones Científicas de la Prov. de Buenos  
Aires (CIC-PBA) & Instituto PLADEMA, Universidad Nacional  
del Centro, Tandil, Argentina.

M. Vénere  
Comisión Nacional de Energía Atómica (CNEA) & Instituto  
PLADEMA, Universidad Nacional del Centro, Tandil, Argentina.

N. Pirró  
Digestive Surgery Department, Hôpital La Timone, Marseille,  
France.

M-E. Bellemare  
LSIS UMR CNRS 7296, Aix-Marseille University, Marseille,  
France.

**Keywords** Deformable models · Segmentation  
framework · Multi-Object Segmentation · Complex  
Segmentation · Collision Control

## 1 Introduction

Nowadays the different medical image modalities aid to immeasurable improvements in the diagnosis and

analysis of several patients conditions. In the last three decades, computer aided diagnosis (CAD) systems have become one of the major research areas in medical imaging and diagnostic radiology (Doi, 2005). Image segmentation plays an essential role in the field of image analysis for CAD systems, being a fundamental stage that determines the eventual success or failure of the later process such as visual inspection, surgical planning, treatments or simulation. However, segmenting anatomical or functional structures from medical images is a challenging task mainly due to different image artifacts, and the complexity of datasets.

Various image analysis tasks require multiple adjacent structures segmentations, for instance, multiple organs in 3D abdominal CT like liver, spleen, kidneys, pancreas and aorta (Okada et al, 2012); brain tumor segmentation, which comprehends white and gray matter, tumor and edema (Yang et al, 2013); pelvic organ prolapse, including segmentation of rectum, bladder and uterus (Bay et al, 2011), among others. Also, other challenging tasks demand complex structure segmentations such as: skull stripping in MRI (Liu et al, 2013), where the different structures of the brain are segmented; knee 3D MRI bone segmentation (Dodin et al, 2011), in which different complex shaped structures may appear; and uterus delineation in dynamic MRI (Namias et al, 2014a) that suffers from inhomogeneities and noise.

Several works have been proposed to resolve particular structure segmentation problems, and significant effort has been dedicated to the improvement of segmentation algorithms. Nevertheless, there are still challenging research directions on the integration of individual snake models for delimiting a single region of interest (ROI) or a group of different ROIs. Chen and Metaxas (2005) have presented a hybrid segmentation framework based on deformable models, where a global energy function is introduced to combine prior-shape, region-based and boundary techniques under a fixed schema for 3D brain image segmentation. Abe and Matsuzawa (2000) have proposed to use multiple active contour models (ACM) that compete with each other to segment a single object of uniform image properties as a set of subregions. More recently, Gao et al (2012) have developed a 3D multi-object segmentation tool, which not only grants mutual exclusion between regions but also parallel segmentation and models interaction using a principle of action and reaction. The authors introduce a novel active contour formulation for that particular framework which allows to segment multiple structures but with a fixed interaction scheme for all the ROIs that limits its flexibility. Additionally, most of the proposed works focus just on

multiple objects detection or complex structures segmentation, not both simultaneously.

Under level sets formulations, Shang et al (2008) have developed a region competition active contour model. The algorithm is derived by minimizing a region based probabilistic energy function and implemented in a level set framework. The model combines edge and region features in a level set evolution equation and has been extended to 3D medical structure detection. A limitation of this approach is that the competing regions are only two: the ROI and the background. Other authors (Vu et al, 2013) have used variations of the Chan-Vese formulation (Chan and Vese, 2001) to segment the image in more than one object plus the background searching for homogeneous intensity regions. Nevertheless, this hypothesis does not hold for some medical imaging modalities because two distinct organs can present similar intensities.

The present paper proposes an open-source segmentation framework named Deformable Models Array (DMA), to be used for medical segmentation tasks involving multiple and complex objects detection. For this purpose, DMA enables using a combination of existing or new explicit deformable models (DM) in an efficient and transparent way. Thus, DMA allows considering several segmentation strategies, for instance, simple segmentation (one ROI only), multiple-object segmentation (simultaneous detection of several ROIs, adjacent or isolated), and complex-object segmentation (ROI with complex shape or different image characteristics), including a novel model cooperative interaction scheme. The framework can deal with image data in both 2D and 3D scenarios and one of its main advantages is the possibility to easily include a set of DM algorithms to quickly develop and test segmentation strategies in almost any existing medical imaging modality.

## 2 Methods

In order to be extensible and adaptable to diverse segmentation problems, the framework must deal with different images modalities (e.g. MRI, CT, etc...), and dimensions: 2D and 3D. Although there is not a segmentation technique which can achieve high quality results in any scenario, the correct election of existing state-of-the-art techniques or the development of a particular new method, could solve this issue. Explicit deformable models have several advantages, specially for parallel and interacting segmentation since their capability to incorporate control mechanism such as evolution restrictions, collision detection, shape guidance, etc.

Moreover, DMA can deal with several segmentation strategies thanks to its ability to use several DM in a cooperative way. Therefore, one of the main contributions of DMA is its *Evolution Control* module, which was specially designed for this purpose. The framework is open-source, implemented mainly as filters over the ITK libraries (Yoo et al, 2002) and its graphical user interface in Qt. ITK has become one of the most complete open-source medical image processing library adding new state-of-the-art techniques in each new release version. The sources are publicly available<sup>1</sup>. In the following, we describe the general DMA formulation and its main components.

## 2.1 Global Scheme

The required input data comprises the image to segment, a set of initial models, called evolving models ( $e_M$ ), and a set of deformable model techniques ( $dm_T$ ) to evolve the  $e_M$ , as well as the parameters of each  $dm_T$ . Hence, these two items are grouped in tuples ( $e_M, dm_T$ ), one for each ROI. Next, DMA enables to use previous segmentation knowledge representing a set of spatial restrictions named as fixed models ( $f_M$ ). Finally, a few framework parameters, later described, must be set to run the segmentation. Consequently, a convenient GUI was designed using the Qt libraries (Blanchette and Summerfield, 2006) to facilitate the DMA experiment set-up, enabling to save and load the complete project state, visualize the scene, etc.

The framework is composed by a set of functional modules. The *Evolution Control* (*EvCtrl*) module is the main component which comprises the novel cooperative functionality, and governs the evolution process. Its three main interrelated tasks are: the evolution process, the collision detection and the state management. A *collision detector* (*ColD*) module is used to evaluate whether any *inter* or *intra*-collision occurs during the models evolution. We consider a collision as the intersection of two or more non-neighbouring elements in the geometrical model representation. As this task has high computational overhead, particularly in 3D, an efficient ad-hoc classification technique was implemented. In addition, a *safe-state* (*SS*) module is considered one for each  $e_M$ , which keeps a history of previous model states and the last known state without collisions. This module is crucial, as it determines whether to continue the evolution of the models. A *collision resolution* (*ColR*) module is concerned with solving the presence of collisions, interacting with each  $dm_T$  to solve these in-

tersections. Finally, we obtain the segmentation result represented by the final state of each input  $e_M$ .

The global segmentation process is shown in Figure 1. The image of interest together with the models initialization are provided to the algorithm: in green the  $e_M$ , and in red the  $f_M$ . The *EvCtrl* module governs the evolutions and interactions of the models until they finish the segmentation process. Finally, if a complex structure segmentation takes place, the post-processing assembles the models comprising the final complex structure.

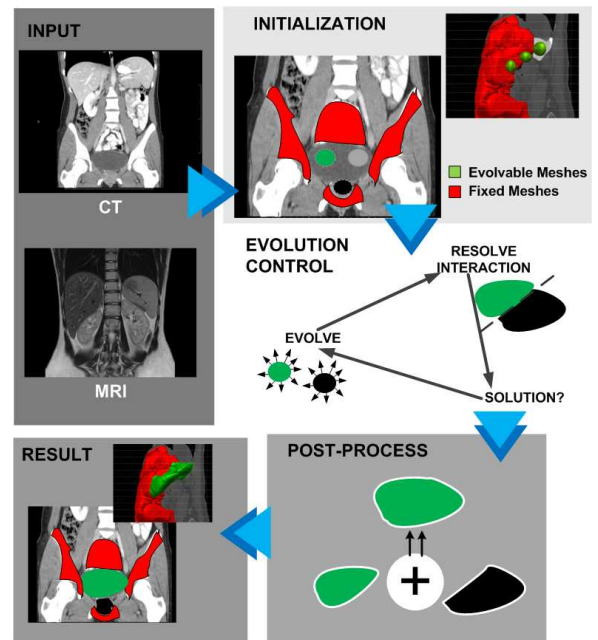


Fig. 1 DMA global segmentation process.

## 2.2 Modules

### 2.2.1 Evolution Control

The *EvCtrl* module is the main coordinator of the segmentation process. Its main task is to synchronize all the  $dm_T$  and control their interactions. Its inputs are the above presented elements:  $e_M + f_M$  models, the  $dm_T$  with all their parameters, the input image and a *synchronization distance* parameter  $N \in \mathbb{N}^+$ . Each  $e_M$  has one instance of an *SS* module, and one instance of the  $dm_T$ . The *SS* keeps a history of previous states of its particular  $e_M$ , and will be able to restore its state to the last collision-safe state or *checkpoint* whenever is required by the *EvCtrl*. The  $dm_T$  guides the  $e_M$  evolution across the iterations. The last *EvCtrl* part is the *ColD* module. This module tracks the  $e_M$  evolutions and in-

<sup>1</sup> [http://www.cifasis-conicet.gov.ar/namias/Files/Filters/DMA\\_Framework\\_Qt5.tar.gz](http://www.cifasis-conicet.gov.ar/namias/Files/Filters/DMA_Framework_Qt5.tar.gz)

teractions, looking for collisions between or inside each  $e_M$ .

The *EvCtrl* module first calls the *ColD* to check for initial collisions and the *SS* module to save the first safe states. Then the evolution loop starts: every  $dm_T$  do  $N$  iterations, consequently the *ColD* checks for collisions and if any occurs the *EvCtrl* ask the diverse  $dm_T$  to solve the collision problems. Finally, the new *checkpoint* is saved in the *SS* module. The loop continues until all  $dm_T$  finish their evolution.

We define *context information* as the knowledge provided by the model interaction, generally as a spatial restriction coming from both the  $f_M$  and the  $e_M$  during the segmentation process under the framework formulation.

### 2.2.2 Safe States

The *SS* module keeps a list of  $e_M$  states along with the iteration number when it is saved, and the last collision-free state or *checkpoint*. The *SS* uses these saved states to restore the models to a safe configuration before mesh overlapping. During evolution, whenever it is necessary, the *EvCtrl* can rollback the  $e_M$  to any of the saved states, apply a collision solution to the problematic nodes, and re-evolve the  $e_M$  towards the current synchronization point.

### 2.2.3 Collision Detector

This module implements a collision detector algorithm. The algorithm concerns with the detection of intersecting elements from different models or elements of the same model (self-collisions). It is worth noting that if a collision is not solved, the segmented models are invalid, as the meshes are struggling or overlapping. Hence, a collision detector should search potential elements in conflict efficiently and, if a collision is detected, some resolution strategy should be taken. Elements collision checking is performed several times, almost for every iteration, adding a high computational cost to the process.

As the collision detector is mainly dependent on the snake model representation, it is important to consider the space dimension to instantiate the particular *ColD*. Therefore, in 2D it is necessary to implement a segment intersection routine, but if we are dealing with a 3D space, the algorithm must handle spatial triangle intersections.

### Improved Collision Detection Strategies:

In real time solutions, grids or kd-trees are good approaches to find elements in space. Some works consider that initial meshes are distant from each other and many evolution steps are required before a collision appears. Nevertheless, this assumption is not completely true, and collisions should be checked every a small number of step, with a high computational cost, even with classifications schemes. Generally, the detection time is higher than the snake evolution time.

A simple strategy to reduce the computational cost even more is to do one collision check after a fixed number of evolution steps  $N$ . If a collision is detected at the end of the interval, the *EvCtrl* goes back to a safe state, resolves the collision and continues. However, if  $N$  is large, intersections could be detected distant from the actual collision iteration. When this occurs, models trends to distort. On the contrary, if  $N$  is small, the computational cost is high; Nonetheless, the borders proximity is tighter. This checking strategy has a collision checking cost of  $\Theta(\frac{K}{N})$  where  $K$  is the total number of evolution steps.

To improve the collision detection algorithm, we implemented another strategy called *sub-step checking*. We still check for collisions each  $N$  steps but saving all the intermediate states (element positions and forces). If no collisions are detected after  $N$  steps, these states are erased. Otherwise, we use a binary search through the saved states to efficiently find the first collided state iteration. Thus, the total detections required for the *sub-step checking* strategy is  $\Theta((K \log N)/N)$ .

### 2.2.4 Collision Resolution Strategies

The final module implements a collision resolution strategy in collaboration with the  $dm_T$  involved to avoid further intersections.

A simple but effective method to solve collisions is to *freeze* colliding elements. These elements are marked, and they are no longer updated in the next evolution steps. Another option, instead of freezing elements, is to use a proportional repulsive force opposite to the movement of each colliding element (Teschner et al, 2005). Even though it is a more general approach, it is unstable, and, in the studied cases leads to a similar result as the freezing strategy, and at a higher cost.



### 3 Results

#### 3.1 Experiments

We introduce five challenging real-case medical segmentation examples where the framework capabilities are highlighted. The first example is a 2D segmentation problem involving multiple and complex pelvic organs in MRI. The uterus borders have low contrast and its inner region has high signal inhomogeneities making it very difficult to segment using a single DM. Namias et al (2014a) remark the segmentation for this problem. Second, two segmentation tasks of adjacent volumetric objects are included: heart segmentation in CT and brain tumor segmentation in MRI. On the one hand, the soft tissue in CT imaging has low contrast making it complicate to segment by common  $dm_T$ . On the other hand, DMA enables to segment multiple tumors simultaneously. Finally, two segmentation examples of complex structures in CT are shown where the presence of obstructing matter completely changes the image intensity inside the ROI.

We have considered two traditional  $dm_T$  for the experiments: T-Snakes McInerney and Terzopoulos (2000) and GVF-Snakes Xu and Prince (1997), which are briefly described in the ‘‘Appendix’’, since their capabilities and previous experience of the authors. The experimental parameters are summarized in Table 1. The experiments were ran in an Intel(R) Core(TM) i5-3570 CPU @ 3.40GHz with 16Gb RAM and Linux kernel version: 3.11.0-23-generic.

The segmentation results are validated against the ground truth (GT) given by the physician or available online. For the 2D experiments we use the Dice similarity coefficient:

$$\mathcal{D}(A, B) = \frac{2 \times |A \cap B|}{|A| + |B|} \quad (1)$$

where  $A$  is the reference pixel set and  $B$  is the DMA resulting pixel set. To compare the 3D surfaces we directly evaluate the volumetric differences using a ray-cast technique over the triangular meshes models according to the following volumetric coefficient metric:

$$\mathcal{M}(A, B) = 1 - (f_n + f_p) \quad (2)$$

$$f_n = \frac{V_{A/B}}{V_A \cup V_B} \text{ and } f_p = \frac{V_{B/A}}{V_A \cup V_B} \quad (3)$$

where  $f_n$  is the false negative rate,  $f_p$  is the false positive rate,  $V_A$  is the volume of the reference model  $A$  and  $V_{A/B}$  is the volume difference between  $A$  and  $B$ . In a similar way,  $V_B$  is the volume of the DMA resulting model  $B$  and  $V_{B/A}$  is the volume difference between  $B$

and  $A$ . Both quality metrics lie between 0 and 1 where 0 means no similarity and 1 a total similarity. With the only purpose of presenting the framework capabilities in the following experiments, we used a manual initialization. Even tough automatic model initialization could be done for each specific case, this issue is out of the scope of this paper.

#### 3.2 Multiple organ segmentation in dMRI (2D)

In this section we present the segmentation of two adjacent pelvic organs: bladder and uterus vagina set (UV-S), under *T2-weighted* dynamic Magnetic Resonance Imaging (dMRI) for prolapse diagnose. The dataset was acquired with informed consent of the patients, taken in the sagittal midline by specialists at the Hôpital La Timone, Marseille, France (Pirro et al, 2009) also used in (Rahim et al, 2010) and (Namias et al, 2014a). The segmentation stage comprises a fundamental part in the MoDyPe project<sup>2</sup> supported by the French National Research Agency under reference ANR-09-SYSC-008. In *T2-weighted* images, the uterus segmentation represents a challenging goal due to its heterogeneous boundary and narrow shape (Namias et al, 2014a).

An initialization example is shown in Figure 2. We use previous segmentations of the the rectum as *context information* (Figure 2, on the right). We use only one  $e_M$  for the bladder and three for the UV-S representing the uterus body, the cervix and the vagina. All  $dm_T$  are T-Snakes. The UV-S set delimitation is particularly difficult because of its intensity inhomogeneities. For this reason we employ a three  $e_M$  set to segment this complex structure. The UV-S region is represented by the union of the  $e_M$  final states.

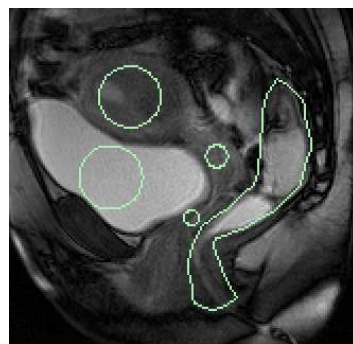


**Fig. 2** Uterus and bladder segmentation in sagittal midline MRI.  $e_M$  (circles on the left) and  $f_M$  (right).

<sup>2</sup> <http://modype.lsis.org>

| Case                      | Input Meshes  | Image                | DMA Parameters                    |
|---------------------------|---|----------------------|-----------------------------------|
| Pelvic organ segmentation | Uterus: $e_M=3$ Bladder: $e_M=1$ , $f_M=2$ (fat, rectum)      | T2 256x256 MRI DICOM | T-Snakes, 2D <i>ColD</i> (N=25)   |
| Heart segmentation        | Heart: $e_M=1$ , $f_M=6$ (lungs, liver, cava, aorta, stomach) | 512x512x167 CT DICOM | T-Snakes, 3D <i>ColD</i> (N=25)   |
| Tumor segmentation        | Tumor: $e_M=1$ , $f_M=2$ (white and gray matter)              | 128x128x90 MRI DICOM | GVF-Snakes, 3D <i>ColD</i> (N=15) |
| Colon segmentation        | Missing sections: $e_M=2 \sim 3$ , $f_M=2$ (colon sections)   | 512x512x562 CT DICOM | T-Snakes, 3D <i>ColD</i> (N=25)   |
| Stomach segmentation      | Stomach: $e_M=3$  | 512x512x218 CT DICOM | GVF-Snakes, 3D <i>ColD</i> (N=15) |

**Table 1** Experiments configuration and parameters.

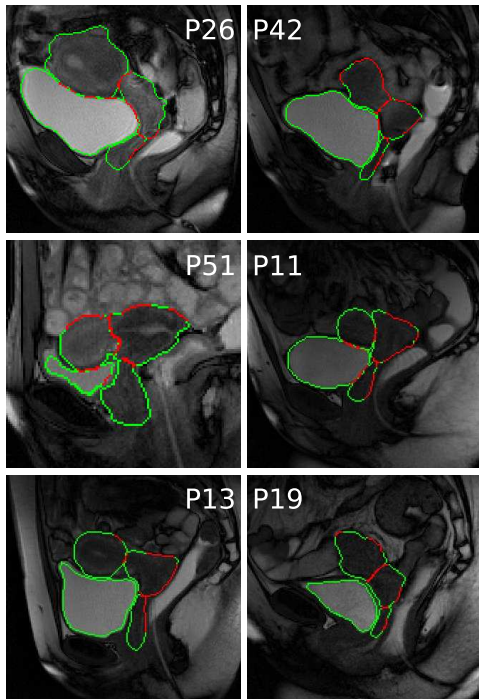


**Fig. 3** Bladder and UV-S final DMA results in six patients. In red the collided segments, in green the non collided.

*Results* We include six patients. This multi-object segmentation experiment exploits most of the capabilities of the framework. Firstly, we segment the bladder and the UV-S simultaneously, using the prior rectum segmentations as constraints. Some qualitative results are shown in Figure 3. In green, the segments that did not collide are depicted, and in red the collided elements. On the one hand, the bladder contours are mostly green as they rarely interact with the UV-S contours. On the other hand, the UV-S borders interact with each other and with the rectum constraint (on the right). Although the  $f_M$  are omitted in the figure, they were considered as constraints. Dice coefficients of the segmentation results against the GT given by the physician are summarized in Table 2. As can be seen, DMA achieves excellent

results, particularly in the UV-S, despite the images intrinsic difficulties.

|     | Bladder | UV-S  |
|-----|---------|-------|
| P11 | 0.967   | 0.864 |
| P13 | 0.936   | 0.871 |
| P19 | 0.957   | 0.862 |
| P26 | 0.942   | 0.855 |
| P42 | 0.921   | 0.882 |
| P51 | 0.865   | 0.920 |

**Table 2** Multiple organs segmentation, quantitative comparison using Dice similarity against GT.

### 3.3 Context Information Evaluation

The next two experiments highlight the importance of the *context information* derived from DMA formulation.

#### *Heart segmentation in CT*

In this experiment, we use a public dataset from the *3D Image Reconstruction for Comparison of Algorithm Database*<sup>3</sup> (Soler et al, 2012) called 3D-IRCADb-02, which is composed of two anonymized abdominal enhanced 3D CT-scans. The first acquisition has been made during the arterial phase in inhaled position. The dataset provides the ground truth segmentation of the principal organs as DICOM images and also triangular surface meshes. We segment the heart using the ground truth meshes of the surrounding organs (lungs, stomach, liver and vena cava) as constraints. The constraint organ meshes are shown in gray in Figure 4(a), the model initialization in green and the GT in yellow. We present three different runs. The first run sets the parameter configuration leading to a model expansion using no image information

<sup>3</sup> <http://www.ircad.fr/fr/recherche/3d-ircadb-02-fr/>

(nullifying the gradient external force). The second run employs all the standard forces but not the *context information*. Finally, the third run utilizes all of the available information.

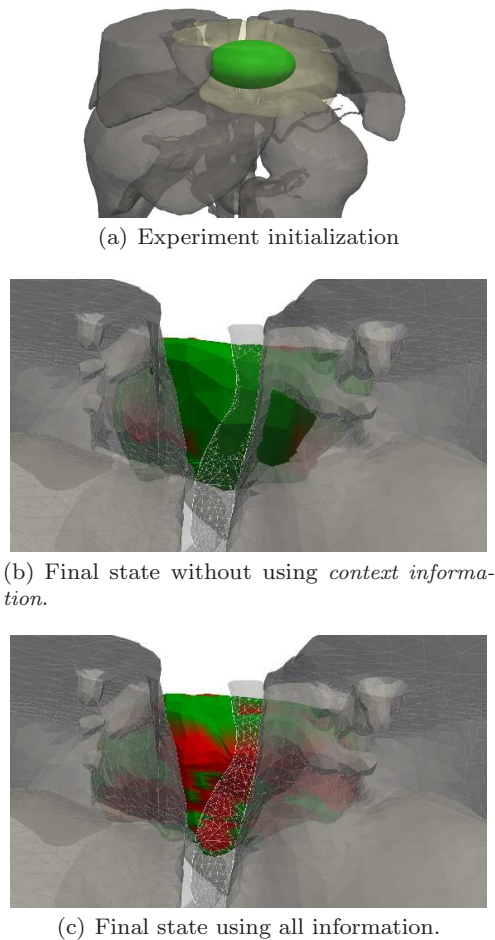


**Fig. 4** Experiment mesh representation. (a) The initial  $e_M$  (in green), ground truth (in translucent yellow) and surrounding organs  $f_M$  (in gray). (b-c) In green the evolving elements and in red the frozen ones for the different runs.

*Results* The first run shows the importance of the *context information* since just using this piece of information, the  $dm_T$  can achieve an acceptable segmentation quality ( $\mathcal{M} = 0.765$ ). As the  $e_M$  does not use image information to guide their evolution, the results should over-segment the heart since the  $e_M$  only stops when it collides with an  $f_M$ . This phenomenon is remarked in the  $f_p$  column of the Context experiment in Table 3. The  $f_p$  representing the over-segmentation phenomenon, depicts the greatest error overall.

In the second run, a standard segmentation is performed. Despite having a better overall segmentation

| Information | $\mathcal{M}$ | $f_p$ | $f_n$ |
|-------------|---------------|-------|-------|
| Context     | 0.765         | 0.183 | 0.052 |
| Image       | 0.845         | 0.089 | 0.066 |
| Both        | 0.892         | 0.075 | 0.033 |

**Table 3** Quantitative comparison of the different information usage during segmentation.

metric ( $\mathcal{M} = 0.845$ ) and half of the  $f_p$  volume compared to the first run, Figure 4(b) shows that the  $e_M$  intersects boundary organs, especially the liver and the stomach.

The final experiment used all of the available information. In this case, the  $e_M$  molded to the surrounding organs (Figure 4(c)), and obtained the best result ( $\mathcal{M} = 0.892$ ) with the lowest  $f_p$  and  $f_n$  volumes.

The analytic results are visually confirmed in Figure 5. Figure 5(a) shows over-segmentation of the DMA result using *context information* (in blue) against the ground truth (in yellow). In Figure 5(b), even though the false positive rate is reduced due to the image information, there are some over-segmented pieces. Finally, Figure 5(c) shows the best result using both image and *context information*.

#### Tumor segmentation in MRI

This experiment consists in tumor segmentation in MRI. Brain tumor image data used in this work were obtained from the *MICCAI 2012 Challenge on Multi-modal Brain Tumor Segmentation*<sup>4</sup> (Landman and Warfield, 2012). We employ four simulated brain MRI from the data set including the simulated image *SimBRATS\_HG0004* which has two tumors (Figure 6). First, we segment the white and gray matter and the meshes are used as *context information* in the experiments. To segment the tumors, the deformable models were initialized with a spheric model (Figure 6(a)) and a GVF-Snake formulation was applied (Figure 6(b)).

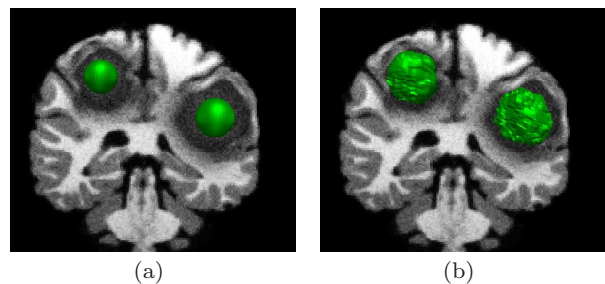


**Fig. 6** MRI tumor segmentation. (a) Experiment set-up. One  $e_M$  for each tumor (green). (c) DMA result.

<sup>4</sup> <http://www.imm.dtu.dk/projects/BRATS2012>



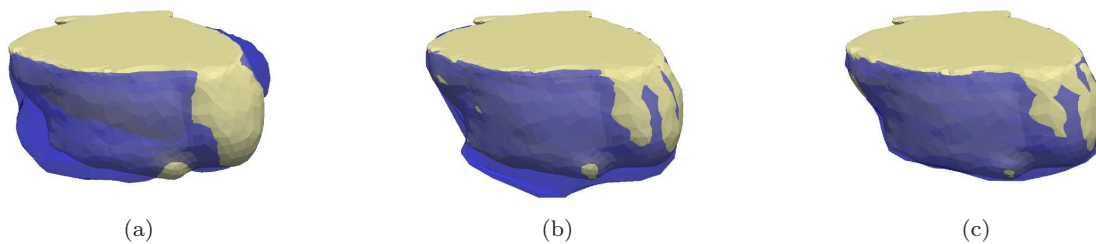


**Fig. 5** segmentation comparison between DMA result (BLUE) and the GT (YELLOW) using: (a) *context information*, (b) image information and (c) DMA image and *context information*

*Results* For the two tumors image, one  $e_M$  was used for each one. We highlight this special case because we could segment both tumors simultaneously using DMA. In this experiment, the usage of *context information* improved the stand alone snake segmentation process as shown in Table 4. As expected, the  $f_p$  is considerably reduced using *context information* what avoids over-segmentation. *Context information* is particularly important in cases where the tumors location context and the extended edema present similar intensities. Under these conditions, the stand-alone snake had lower quality results than DMA ( $4_1$  &  $4_2$ , Table 4).

### 3.4 Obstructions in CT

In CT imaging, some anatomic structures can feature remarkable heterogeneous image intensities. A representative example is the digestive system where there is a mixture of air, liquids, food, and fecal material. Under these circumstances, a simple segmentation strategy fails to properly segment the organ of interest. Nevertheless, the DMA framework can handle this issue. We present two occlusion segmentation examples: colon segmentation and stomach segmentation. A sagittal view of the rectum in a CT Colonography (CTC) is shown in Figure 7(a). Feces, rather than dark(air), appear in the rectum with a brighter signal intensity hampering the segmentation task. A sagittal view of the stomach is depicted in Figure 7(b). Likewise, the presence of food, liquids and air produces two distinctive signal intensities.

#### *Colon segmentation*

In this case, we use an anonymized public colonoscopy computed tomography (CTC) image from the National Cancer Institute Image Cancer Archive <sup>5</sup>.

Some images present obstructions because of liquid and

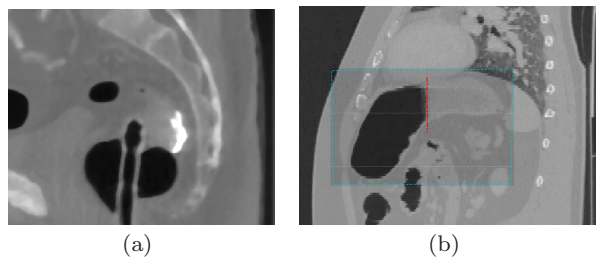


**Fig. 7** Occlusion examples in CT. (a) Rectum occluded region in a CTC. (b) Stomach occluded region from the IRCAD dataset. Heterogeneous region limit in red line

fecal matter. These obstacles lead the automatic segmentation algorithm to fail. Two experiments are depicted in Figure 8. In red, the previous segmentation result of the algorithm described in Namias et al (2014b) and DMA  $e_M$  initialization in green, respectively. The problematic regions have a noisy decaying intensity signal and narrow shapes. Therefore, we initialized the ROI with multiple T-Snakes models. The final meshes configuration is shown in the right column.

*Results* DMA was applied in 5 CTCs of the dataset where different sections were obstructed. No quantitative measures are presented because the missing found portions are about 4% ~ 8% of the total volume of the ROI, giving a minimum variation of the  $\mathcal{M}$  index ( $\sim 0.05\%$ ). In all cases, DMA managed to complete and connect the pending sections (Figures 8(a) and 8(b) on the right).

#### *Stomach segmentation*

The second occlusion experiment also uses the acquisitions from the 3D-IRCADb-02 dataset. We segmented the stomach in two images. In both cases we set three  $e_M$ , two for the dark region and one for the bright one as shown in Figure 9(a). No *context information* was used.

*Results* Table 5 summarizes the segmentation results. DMA achieves good results in both cases, even though

<sup>5</sup> <http://cancerimagingarchive.net/>

| Data Set       | No Context    |       |       | With Context  |       |       |
|----------------|---------------|-------|-------|---------------|-------|-------|
|                | $\mathcal{M}$ | $f_P$ | $f_N$ | $\mathcal{M}$ | $f_P$ | $f_N$ |
| 1              | 0.867         | 0.019 | 0.114 | 0.936         | 0.003 | 0.061 |
| 2              | 0.848         | 0.022 | 0.130 | 0.890         | 0.002 | 0.108 |
| 4 <sub>1</sub> | 0.593         | 0.365 | 0.042 | 0.879         | 0.003 | 0.118 |
| 4 <sub>2</sub> | 0.682         | 0.265 | 0.053 | 0.843         | 0.005 | 0.152 |
| 7              | 0.832         | 0.121 | 0.049 | 0.895         | 0.003 | 0.102 |

**Table 4** Tumor segmentation experiment. Context information vs. stand alone snake technique.

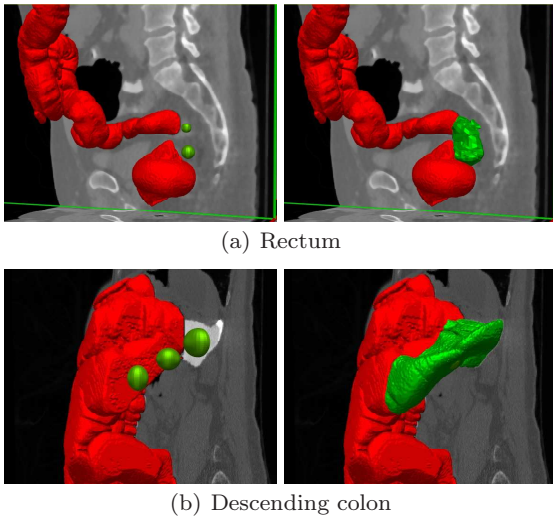


**Fig. 8** CTC colon obstruction problems. Experiment set-ups on the left. Previous segmentation results (in red) acting as  $f_M$ . The  $e_M$  in green. Mesh representation of the segmentation result over the CT on the right.

there are high  $f_n$  rates because the method under-segments the ROI. A sagittal view of the segmentation result is presented in Figure 9(c). The dotted lined circles show where the under-segmentation occurs, being the most difficult areas to include because of intensity variations, concave shape and models interaction that make models stop distant from the real borders.

| Case     | $\mathcal{M}$ | $f_P$ | $f_N$ |
|----------|---------------|-------|-------|
| IRCAD2.1 | 0.890         | 0.006 | 0.104 |
| IRCAD2.2 | 0.865         | 0.003 | 0.132 |

**Table 5** Stomach segmentation performance.

## 4 Discussion

The real-case experiments included several segmentation strategies available on DMA. For instance, simple segmentation with constraints (heart), multiple segmentation (tumors) and complex segmentation (stomach and colon) and both complex and multiple segmentation (pelvic organs) which included CT and

MRI imagery in 2D and 3D, and multiple  $dm_T$ , showing the adaptability and wide branch of potential applications for the framework.

More precisely, in the uterus and bladder example, we segmented both a complex structure and a simple one simultaneously. The  $e_M$  evolved in parallel and competed against each other to advance towards the organs borders. In the heart and tumor experiments, we simulated a sequential segmentation where we used previous knowledge such as  $f_M$  to evaluate the importance of the contextual information. The DMA results show that the *context information* improved the stand alone snake results reducing the false positive rate, but sometimes increasing the false negative error. Then, we presented a concrete segmentation application where the DMA formulation is specially advantageous. We introduced two examples including colon and stomach segmentation in CT with obstruction problems. We took advantage of the framework characteristics to straightforwardly solve complex structure segmentation scenarios where previous works needed two or more different segmentation steps. A fair comparison between DMA and existing methods is hard because the latter cannot not model these complex scenarios as a whole.

In all cases, collision detection plays an outstanding role. Mesh collisions are detected and managed, both in 2D and 3D using different image modalities. It provides the usage of previous knowledge, in the form of meshes, as spatial restrictions to the  $e_M$ . The explicit use of *context information* is a contribution since no previous works stand out its importance and benefits.

## 5 Conclusion

A novel open-source framework for multi-object segmentation in medical images was presented. The framework allows using and combining any explicit deformable model technique to perform segmentation tasks under different modalities in a transparent way. One of the main contributions of this proposal is the incorporation of a control scheme to coordinate the evolution of

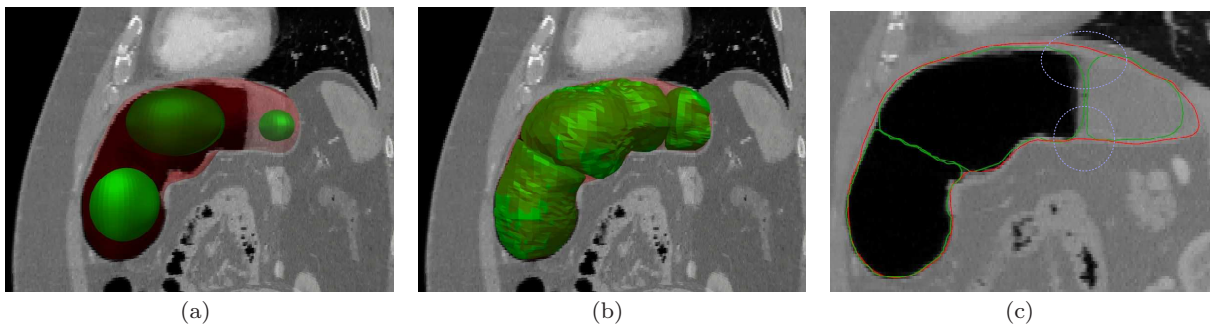


**Fig. 9** Stomach segmentation experiment over complex structure ROI. (a) Experiment set-up over the CT. In translucent red the GT, in green the  $e_M$  initialization. (b) DMA segmentation result. (c) Under-segmentation problems.

the models and resolve interaction issues. This module not only helps to prevent object overlapping or leakage, but also provides a mechanism to introduce context information from the other ROIs as fixed models. This piece of information has an important relevance since it improved, in some occasions, the standalone techniques segmentations results. Other relevant contribution is its possibility to work under several segmentation conditions: sequentially, by first segmenting the “simple” objects, converting them to fixed models and then “hard” ones; or, in parallel, evolving multiple models that compete to segment different ROIs. The experimental results showed great adaptability to a wide range of medical imaging scenarios.

Although only two classic  $dm_T$  were employed, DMA can easily integrate any explicit method. Moreover, for the collision resolution module, other strategies could be incorporated, which should be considered as future work. Nevertheless, we think that using, for instance, a repulsion force, would lead to similar results increasing the computational cost.

## Appendix: Snakes Formulations

Snakes are explicit deformable models that can evolve towards an object boundary within the image under the influence of internal forces and external forces. After the initial proposal of Kass et al (1988), several formulations have been proposed (He et al, 2008). In this paper, we consider two well-known DM techniques as examples. The first method is based on the T-Snakes formulation proposed by McInerney and Terzopoulos (2000) and the second is the Gradient Vector Flow Snakes (GVF-Snakes) presented by Xu and Prince (1997).

### 5.1 T-Snakes formulation

T-Snakes based methods are discrete approximations to a conventional parametric snakes model while retaining many of its properties. The model is geometrically represented by a closed polygonal for 2D problems and by a triangular surface mesh for 3D. The deformation of the snake model is governed by discrete Lagrangian equations of motion, and each element  $\mathbf{x}(t)$  evolves according to the following motion equation:

$$\mathbf{x}(t+1) = \mathbf{x}(t) - \Delta t (a\alpha(t) + b\beta(t) - p\rho(t) - q\mathbf{f}(t)) \quad (4)$$

where  $\alpha$ ,  $\beta$  are the internal forces (tension and flexion),  $\mathbf{f}$ ,  $\rho$  are the external forces (balloon and image gradient forces), and  $a$ ,  $b$ ,  $p$  and  $q$  are the force weighting parameters.

The T-Snakes formulation modifies the original external force adding an adaptive inflation force  $\rho(t)$  term depending on the image intensity features.

$$\rho(t) = F(I(x(t))) \cdot \mathbf{n}(x(t)) \quad (5)$$

where  $\mathbf{n}$  is the unitary normal vector to the model and  $F$  is a binary function relating  $\rho$  to the intensity field of the image  $I$ :

$$F(I(x(s,t))) = \begin{cases} +1 & \text{if } \frac{|I(x(s,t)) - CI(r)|}{k\sigma(r)} \leq 1 \\ -1, & \text{otherwise} \end{cases} \quad (6)$$

where  $CI(r)$  is the characteristic intensity of the ROI,  $\sigma(r)$  is the ROI intensity deviation, and  $k$  is an input parameter.

### 5.2 GVF-Snakes formulation

Gradient vector flow (GVF) snakes introduce a new external force for active contour models. The difference between traditional snakes and GVF-Snakes consists in that the latter converge to boundary concavities and

they do not need to be initialized close to the boundary (Xu and Prince, 1997).

To improve the original snake formulation, the authors introduced a non-irrotational external force field  $v(x, y) = [u(x, y), v(x, y)]$  known as gradient vector flow field. The field is calculated as a diffusion of the gradient vectors of a gray-level or binary edge map:

$$GVF = \iint \mu(u_x^2 + u_y^2 + v_x^2 + v_y^2) + |\nabla f|^2 |v - \nabla f|^2 dx dy \quad (7)$$

where  $\mu$  is an input parameter.

## References

- Abe T, Matsuzawa Y (2000) A region extraction method using multiple active contour models. In: Computer Vision and Pattern Recognition, 2000. Proceedings. IEEE Conference on, IEEE, vol 1, pp 64–69
- Bay T, Chambelland JC, Raffin R, Daniel M, Bellemare ME (2011) Geometric modeling of pelvic organs. In: Engineering in Medicine and Biology Society, EMBC, 2011 Annual International Conference of the IEEE, IEEE, pp 4329–4332
- Blanchette J, Summerfield M (2006) C++ GUI programming with Qt 4. Prentice Hall Professional
- Chan T, Vese L (2001) Active contours without edges. IEEE Transactions on Image Processing 10(2):266–277
- Chen T, Metaxas D (2005) A hybrid framework for 3d medical image segmentation. Medical Image Analysis 9(6):547–565
- Dodin P, Martel-Pelletier J, Pelletier JP, Abram F (2011) A fully automated human knee 3d MRI bone segmentation using the ray casting technique. Medical & biological engineering & computing 49(12):1413–1424
- Doi K (2005) Current status and future potential of computer-aided diagnosis in medical imaging. The British Journal of Radiology 78(suppl1):s3–s19
- Gao Y, Kikinis R, Bouix S, Shenton M, Tannenbaum A (2012) A 3d interactive multi-object segmentation tool using local robust statistics driven active contours. Medical image analysis 16(6):1216–1227
- He L, Peng Z, Everding B, Wang X, Han C, Weiss K, Wee W (2008) A comparative study of deformable contour methods on medical image segmentation. Image and Vision Computing 26(2):141–163
- Kass M, Witkin A, Terzopoulos D (1988) Snakes: Active contour models. International Journal of Computer Vision 1(4):321–331
- Landman B, Warfield S (2012) Miccai 2012 workshop on multi-atlas labeling. In: Medical Image Computing and Computer Assisted Intervention Conference 2012: MICCAI 2012 Grand Challenge and Workshop on Multi-Atlas Labeling Challenge Results
- Liu HT, Sheu TW, Chang HH (2013) Automatic segmentation of brain MR images using an adaptive balloon snake model with fuzzy classification. Medical & biological engineering & computing 51(10):1091–1104
- McInerney T, Terzopoulos D (2000) T-snakes: Topology adaptive snakes. Medical Image Analysis 4(2):73–91
- Namias R, Bellemare ME, Rahim M, Pirr o N (2014a) Uterus segmentation in dynamic MRI using lbp texture descriptors. In: SPIE Medical Imaging, International Society for Optics and Photonics, pp 90,343W–90,343W
- Namias R, D’Amato J, del Fresno M, V enere M (2014b) Automatic rectum limit detection by anatomical markers correlation. Computerized Medical Imaging and Graphics 38(4):245 – 250
- Okada T, Linguraru MG, Hori M, Suzuki Y, Summers RM, Tomiyama N, Sato Y (2012) Multi-organ segmentation in abdominal ct images. In: Engineering in Medicine and Biology Society (EMBC), 2012 Annual International Conference of the IEEE, IEEE, pp 3986–3989
- Pirro N, Bellemare M, Rahim M, Durieux O, Sieleznoff I, Sastre B, Champsaur P (2009) R esultats pr eliminaires et perspectives de la mod elisation dynamique pelvienne patient-sp ecifique. Pelviperin eologie 4(1):15–21
- Rahim M, Bellemare ME, Bulot R, Pirr o N (2010) Pelvic organs dynamic feature analysis for MRI sequence discrimination. In: Pattern Recognition (ICPR), 2010 20th International Conference on, IEEE, pp 2496–2499
- Shang Y, Yang X, Zhu L, Deklerck R, Nyssen E (2008) Region competition based active contour for medical object extraction. Computerized Medical Imaging and Graphics 32(2):109–117
- Soler L, Hostettler A, Agnus V, Charnoz A, Fasquel J, Moreau J, Osswald A, Bouhadjar M, Marescaux J (2012) 3d image reconstruction for comparison of algorithm database: A patient-specific anatomical and medical image database
- Teschner M, Kimmerle S, Heidelberger B, Zachmann G, Raghupathi L, Fuhrmann A, Cani MP, Faure F, Magnenat-Thalmann N, Strasser W, et al (2005) Collision detection for deformable objects. In: Computer Graphics Forum, Wiley Online Library, vol 24, pp 61–81



- Vu D, Ha T, Song M, Kim J, Choi S, Chaudhry A (2013) Generalized chan-vese model for image segmentation with multiple regions. *Life Science Journal* 10(1):1889–1895
- Xu C, Prince JL (1997) Gradient vector flow: A new external force for snakes. In: *Computer Vision and Pattern Recognition, 1997. Proceedings., 1997 IEEE Computer Society Conference on, IEEE*, pp 66–71
- Yang H, Zhao L, Tang S, Wang Y (2013) Survey on brain tumor segmentation methods. In: *Medical Imaging Physics and Engineering (ICMIPE), 2013 IEEE International Conference on, IEEE*, pp 140–145
- Yoo TS, Ackerman MJ, Lorensen WE, Schroeder W, Chalana V, Aylward S, Metaxas D, Whitaker R (2002) Engineering and algorithm design for an image processing api: A technical report on itk-the insight toolkit. *Studies in health technology and informatics* pp 586–592

## Biographies



**M. del Fresno** received her PhD (2008) at the UNICEN University (Tandil, Argentina). Currently she is professor in the Department of Computer Science at the same University and member of the Comisión de Investigaciones Científicas de la Provincia de Buenos Aires. Her research interests include medical image processing, segmentation and visualization.



**M. Vénere** is a PhD in Nuclear Engineering from Balseiro Institute, Argentina. He's an Associated Professor in Computer Graphics and Algorithms courses at the UNICEN University (Tandil, Argentina). He is leading several projects in arterial fluid simulation, real time training and computer graphics; among other topics. He is the Co-Director of the PLADEMA Research Institute of the UNICEN University at Tandil, Argentina.



**R. Namias** is a PhD in Computer Science from Rosario National University, Rosario, Argentina, in 2015. He is currently doing a posdoc at Centro Internacional Franco Argentino de Ciencias de la Información y Sistemas (CIFA-SIS). His research interests are in the areas of medical imaging, segmentation, and features analysis.

**N. Pirró** is a digestive system and general surgeon at Hôpital de la Timone in Marseille, France. He is a Professor in Faculté de Médecine - Aix Marseille Université. His research interests are in the areas of pancreatic diseases and pelvic organ prolapse.



**J. P. D'Amato** is Phd in Computational and Industrial Mathematics since 2011 at the UNICEN University (Tandil, Argentina). He's professor assistant in Computer Graphics courses and has worked in the development of real time systems and simulators for the Argentine Army Forces. His main research interests include geometry, high performance in GPUs, visualization and virtual reality applied to training.



**M-E. Bellemare** is a PhD in telecommunication, signal and image processing at Rennes University. He's an Associated Professor in Aix Marseille Université - Polytech' Marseille Dpt GII. His research interests include medical imaging analysis, computer assisted surgery and biomedical engineering.